Received: 4 November 2020 | Revised: 22 March 2021 | Accepted: 11 April 2021

DOI: 10.1002/er.6794

RESEARCH ARTICLE

INTERNATIONAL JOURNAL OF ENERGY RESEARCH WILEY

Energy, exergy, and economic (3E) evaluation of a CCHP system with biomass gasifier, solid oxide fuel cells, micro-gas turbine, and absorption chiller

Junxi Jia[1,3] | **Guiyan Zang**[2] | **Manosh C. Paul**[3]

[1]College of Power and Energy Engineering, Harbin Engineering University, Harbin, China

[2]Department of Mechanical and Industrial Engineering, The University of Iowa, Iowa City, Iowa

[3]Systems, Power and Energy, James Watt School of Engineering, University of Glasgow, Glasgow, UK

Correspondence
Junxi Jia, College of Power and Energy Engineering, Harbin Engineering University, Harbin 150001, China.
Email: jiajunxi99@sohu.com

Manosh C. Paul, Systems, Power and Energy, James Watt School of Engineering, University of Glasgow, Glasgow G12 8QQ, UK.
Email: manosh.paul@glasgow.ac.uk

Funding information
China Scholarship Council

Summary

The aim of this work is to investigate a novel integrated cooling, heating, and power (CCHP) system with biomass gasification, solid oxide fuel cells (SOFC), micro-gas turbine, and absorption chiller. The performance of this system is analyzed by mathematical models consisting of lumped models of SOFC and absorption chiller and one-dimensional model of a downdraft biomass gasifier. Effects of main operating parameters such as moisture content of biomass, air flow rate in the gasifier, and temperature of fuel gas on the overall energy and exergy performance of CCHP system are evaluated. The net present value (NPV) method is used to analyze the economic prospects of this system. The results show that higher flow rate of air for the gasifier with lower moisture content of biomass are beneficial for the improvement of the output of cooling, heating, and power of CCHP, and, accordingly, the electrical efficiency as well as overall energy and exergy efficiency of CCHP rises. Increasing mass flow rate of air for the gasifier can increase exergy efficiency by 10%. Moisture content less than 0.2 could result in exergy efficiency greater than 45% and CCHP efficiency over 65%. The decrease of the exhaust gas temperature further boosts the production of cooling and heating of the CCHP system. Specifically, a 10% improvement of overall efficiency of CCHP is obtained when the exhaust gas temperature is reduced to 90°C. In this work, an electrical efficiency over 50%, exergy efficiency more than 40%, and CCHP efficiency up to 80% can be achieved. Economic assessment shows that the initial investment of SOFC is above 50%-60% of the total investment of the CCHP and the payback period is about 7-8 years.

KEYWORDS

absorption refrigeration, biomass gasification, combined cooling heating and power, solid oxide fuel cell

1 | INTRODUCTION

To meet the world's rising demand for energy supply and to reduce emissions of greenhouse gas (GHG) and air pollution, more efficient and sustainable energy systems are necessary.[1] Combined cooling, heating, and power (CCHP) system is one of the effective ways to reduce the energy consumption and also the GHG emission and

brings about economic benefits. It has already been explored in a wide range of buildings such as farms, distributed neighborhood, universities, airports, hospitals, and supermarkets worldwide.[2] Meanwhile, a CCHP, known as trigeneration, offers an energy supply way with the flexibility to combine renewable energy and energy conversion and storage technologies.[3]

CCHP composed of trigeneration equipment and renewable energy sources has been widely investigated recently. Some of these distributed CCHP systems show high thermal efficiency appromixately 70%-80% compared with conventional energy system such as the large centralized power plant.[4] Among the renewable energy resources, biomass is one of the most promising options for CCHP. Different CCHP systems based on integrating biomass conversion and utilization with power and refrigeration cycles have been proposed and investigated.

Several studies have summarized the technological characteristics of biomass-based CCHP system in recent years.[5] These studies focused on the biomass conversion methods to fuel CHP/CCHP systems.[6] The main conversion methods include combustion, gasification, pyrolysis, biochemical, and chemical processes.[7] Compared with combustion processes, gasification could process lower-grade fuels and extend the range of fuels, and it is more efficient in terms of producing electric power and heat.[8] For the biomass gasification CCHP systems, a downdraft gasifier seems to be more practical for gasification than the updraft gasifier due to the higher quality of syngas and also more cost-effective than the fluidized bed gasifier due to lower maintenance cost.[9]

As for secondary conversion technologies, the working fluid can be steam, combustional gas, or other gaseous fluids. Accordingly steam turbine, organic Rankine cycle (ORC), internal combustion engine (ICE), micro gas turbine (MGT), and fuel cells could be used as a prime mover to meet the target temperatures and power quality. Due to lower initial investment costs and advanced technological developments, ICEs have been applied for small-scale CCHP from 30 kW up to 1000 kW. Yang et al[10] proposed a trigeneration system integrated with biomass-air gasification, ICE, and absorption chiller and carried out the energy and exergy analysis and discussed the economic performance in a biomass trigeneration system. Destruction analyses of energy and exergy indicate that the largest destruction occurs in the gasification system, which accounts for more than 60% of the total energy and exergy losses. The power system studied by Maneerung et al[11] which integrated the downdraft gasifier with ICE shows that the system could achieve an energy efficiency about 32%, whereas the exergy efficiency is 15.6%.

However, the electrical efficiency of CCHP using ICE as a prime mover with 40-100 kW or less than 40 kW nominal power is about 21%-25% which is a bit lower than that based on other prime movers such as gas turbines.[5] Meanwhile, in terms of syngas usage, ICEs are liable to be damaged by lower-quality gases, thus more sophisticated cleaning systems have to be introduced. Micro-gas turbine is another attractive technology for CCHP, ranging from a few kW to several hundreds of kW. They are light in weight and more compact and produce lower noise, vibration, and emission compared with a combustion engine. Numerous research studies have been done to adopt a micro GT as a prime mover in CCHP systems.[12] In the work of Taheri et al,[13] a biomass trigeneration energy system consisting of a combination of biomass gasifier-gas turbine cycle, a Rankine cycle, an absorption chiller, and a proton-exchange membrane fuel cell (PEMFC) is presented for the investigation of power, cooling, and hydrogen production. Thermodynamic performance and total cost rate are studied for the overall system. Their results show that the fuel mass flow rate is the main factor affecting the energy efficiency and total cost rate, and the energy efficiency can reach up to 40%. Yannay et al analyzed the exergo environmental aspects of integrated gasification combined cycle (IGCC) fueled with a municipal solid wastes including a gasifier, gas turbine, and steam turbine. They emphasized that the gasifier is the main factor for improving the overall performance and to reduce the total environmental impact by increasing its exergetic efficiency and reducing the pollutants formation. Zang et al[15] carried out a comparative study of biomass-integrated gasification combined cycle (BIGCC) power systems related to the latest improvements for biomass gasification agents, gas turbine combustion methods, and CO_2 capture and storage options. Through exergy analysis using Aspen Plus, their study shows that the energy efficiency is between 27% and 39% with the exergy efficiency ranging from 22.3% to 37.1%. Their studies found that GTs offer advantages over a reciprocating engine including higher flexibility and efficiency, with lower emissions and electricity costs.

However, micro-gas turbines may suffer great efficiency losses in case of partial load of operation; therefore, sometimes, they are inconvenient for a small-scale distributed CCHP system.[16] Compared with trigeneration system based on heat engines mentioned above, those with fuel cells as a prime mover have merits such as higher efficiency, higher power-to-heat ratio, quitter operation, simple maintenance requirements, lower exhaust emission, and efficient part-load performance.[17] Rokni[18] presented a trigeneration system which was able to produce power, heat, and cool simultaneously at all times based on municipal waste gasification integrated

with SOFC and absorption chiller. The energy efficiency of such small trigeneration system is above 83% and electrical efficiency over 35%. Jia et al[19] investigated an integrated system with a biomass gasifier and SOFC by energy and exergy analyses. A performance comparison with different gasification agents is studied by thermodynamic analysis. For the case where steam as the gasification agent was used, the net electrical efficiency was about 40%. The exergy of combined heat and power efficiency was above 36%, higher than those when air or oxygen-enriched air is used as gasification agent. Other studies also show that the electric efficiency of CCHP based on SOFC can reach 35%-45%,[20] larger than that of 32% as in the case of heat-engine-based CHP.[11]

The SOFC exhaust still has a high temperature, and it can be integrated with a micro-gas turbine to produce additional electricity, which could improve the electrical efficiency of CCHP. Mehdi et al[21] studied an autothermal biomass gasification, SOFC and MGT CHP system. The effects of operating parameters on the electrical and CHP efficiency are calculated. The maximum electric efficiency in their study is 42%. Ghaffarpour et al[22] proposed a system consisting of a gasifier, SOFC, GT, and Rankine cycles. The effects of operating parameters on the thermodynamic and economic performance are investigated. Jia et al also studied a CHP system of biomass gasification with SOFC and micro-gas turbine by thermodynamic model. Electrical and combined heat and power efficiencies increase with decline of moisture content and rising of equivalence ratio; the electrical efficiency of their system could reach over 45% and get a level of up to 56%. Bang et al[24] have reported that BG, SOFC, and MGT hybrid system could obtain an electric efficiency of 58.2%.

The cooling units in CCHP recovering the low-grade waste heat of exhaust gas from prime mover such as micro GT can improve the whole energy efficiency of power system and lead to higher profitability.[25] Compared with vapor-compression systems, liquid instead of vapor is compressed in absorption refrigeration (AR) systems. Accordingly, absorption refrigeration systems have the advantage of relatively small work input than vapor-compression systems and often neglected in the thermodynamic analysis. The AR systems are often classified as heat-driven systems[26] since they are based on heat transfer from an external source. The most widely used two absorption refrigeration systems are the water–ammonia system, where ammonia (NH_3) serves as the refrigerant and water (H_2O) as the transport medium. While for lithium bromide–water (LiBr–H_2O) refrigeration systems, water serves as the refrigerant.[27] To improve its design and operation and economical profit[28] is necessary because the main drawbacks of AR systems compared with compression refrigeration systems are lower efficiency and higher costs.

Due to the diversity of prime movers and the difference of heat recovery units, there are wide varieties of CCHP. According to the best of authors' knowledge, energetic, exergetic, and economic analyses of a biomass-based CCHP system comprising of a downdraft gasifier, SOFC, micro GT, and absorber refrigerator is rare.

Table 1 gives the comparison of this CCHP with some other CCHP systems. It shows that comprehensive performance assessment of the specific CCHP system in this work has not been conducted adequately and need to be studied in detailed.

The main objects and novelties of this work are listed as

- A novel CCHP system composed of a downdraft gasifier, SOFC, micro GT, a single-effect LiBr–H_2O absorption chiller, and hot water heat exchanger is proposed.

TABLE 1 Comparison of the proposed CCHP with other CCHP systems

References	Main Components of System	Fuel	Gasifier Model	Exergy Analysis	Economic Analysis
[21]	SOFC + GT + HSRG	Biomass gas	Lumped equilibrium model	No	No
[22]	SOFC + GT + ST + HSRG	Biomass gas	Lumped equilibrium model	No	Yes
[29]	ICE + ARS	Biomass gas	Lumped equilibrium model	Yes	No
[30]	SOFC + HRU + ARS	H_2	-	Yes	Yes
[31]	SOFC + GT + WH	CH_4	-	Yes	No
[32]	SOFC + GT + ORC	Biomass gas	Lumped equilibrium model	Yes	Yes
This work	SOFC + GT + ARS + HRU	Biomass gas	1-D kinetic model	Yes	Yes

- One-dimensional kinetic model considering both chemical reaction rate and length of reduction zone to overcome the limitations of the lumped equilibrium model of gasifier.
- The overall performance of CCHP is investigated by energetic and exergy analysis, and the net present value (NPV) method is used to assess the economic potential e of this CCHP.

2 | MATHEMATICAL MODELS

The configuration in this work is shown in Figure 1, which is composed of a dryer, gasifier, gas cleaning unit to yield syngas, fuel cell, and micro-gas turbine as a prime mover to produce power, and a single effective LiBr–H_2O absorption chiller to make cooling. A hot water heat exchanger as a heat recovery unit (HRU) is employed to generate domestic hot water.

2.1 | Drying

The initial moisture content of biomass and is set as 40% in this work and is decreased by 5%-25% after leaving dryer.

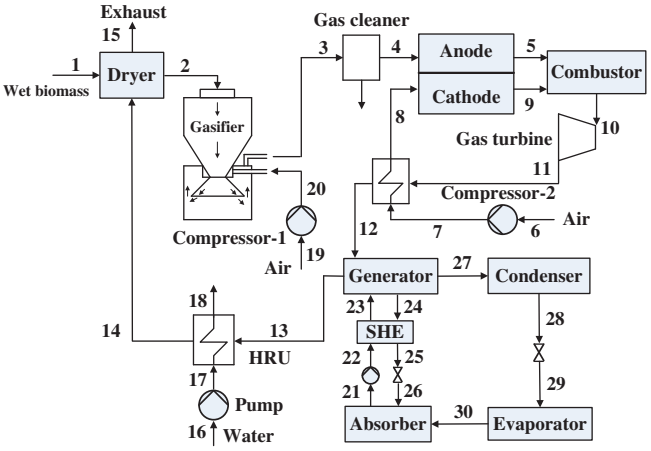

FIGURE 1 Integrated CCHP system with biomass gasifier, SOFCs, micro GT, AR, and HRU [Colour figure can be viewed at wileyonlinelibrary.com]

The ultimate analysis of biomass is shown in Table 2.

The mass balance of drying process is shown as:

$$CH_aO_bN_c + wH_2O_{(l)} = CH_aO_bN_c + w_lH_2O_{(l)} + w_vH_2O_{(v)}. \quad (1)$$

where $a = 1.54$, $b = 0.6255$, and $c = 0.0047$ based on Table 2.

The moisture content (MC) is expressed as

$$MC = \frac{Mass_{water}}{Mass_{total}} = \frac{18w}{12 + a + 16b + 14c + 18w}. \quad (2)$$

Therefore, the heating for wet biomass drying is calculated by

$$Q_{dry} = 2445055 \frac{\dot{m}_{biomass,dry}(MC_1 - MC_2)}{(1 - MC_1)(1 - MC_2)} \quad (3)$$

since at 25°C, the enthalpy of water evaporation for water is 2445.055 kJ kg^{-1} $MC_1 = 0.4$ is the initial moisture content and MC_2 is the moisture content before entering gasifier varying from 0.15 to 0.35 in this work.

2.2 | Gasifier

The dimensions of downdraft gasifier in this study are same as that shown in literature of Jayah et al[34] This downdraft gasifier is divided into two parts: pyrolysis–oxidation and reduction zone.

The global process in the pyrolysis–oxidation zone can be expressed as

$$CH_aO_bN_c + w_lH_2O_{(l)} + m(O_2 + 3.76N_2) = x_1H_2 + x_2CO + x_3CO_2 + x_4H_2O + x_5CH_4 + x_6N_2 + x_7C. \quad (4)$$

The carbon reaction and shift reaction in the pyrolysis–oxidant zone are

$$R1: C + 2H_2 \leftrightarrow CH_4, \quad (5)$$

TABLE 2 Ultimate analysis of biomass[33]

	Ultimate Analysis (On Dry Basis)							Heating Value (MJ kg^{-1})	Enthalpy of Formation (kJ mol^{-1})
Fuel	C	H	O	N	Ash	Fixed Carbon	Volatile Matter	HHV	$\bar{h}_f^0$
Wood	50.6	6.5	42.2	0.28	0.7	19.2	80.1	21.0	119.28

$$\mathrm{R2}: \mathrm{CO} + \mathrm{H_2O} \leftrightarrow \mathrm{H_2} + \mathrm{CO_2}. \tag{6}$$

The heat balance equation can be written as

$$\begin{aligned} &\mathrm{H_{CH_aO_bN_c}} + w\mathrm{H_{H_2O}} + m\mathrm{H_{O_2}} + 3.76m\mathrm{H_{N_2}} \\ &= x_1\mathrm{H_{H_2}} + x_2\mathrm{H_{CO}} + x_3\mathrm{H_{CO_2}} + x_4\mathrm{H_{H_2O}} \\ &\quad + x_5\mathrm{H_{CH_4}} + x_6\mathrm{H_{N_2}} + x_7\mathrm{H_C} + m_{\mathrm{ash}}C_{\mathrm{p,ash}}(T - T_0). \end{aligned} \tag{7}$$

The carbon reactions and steam reforming reaction in the reduction zone are

$$\mathrm{R3}: \mathrm{C} + \mathrm{CO_2} \leftrightarrow 2\mathrm{CO}, \tag{8a}$$

$$\mathrm{R4}: \mathrm{C} + \mathrm{H_2O} \leftrightarrow \mathrm{CO} + \mathrm{H_2}, \tag{8b}$$

$$\mathrm{R5}: \mathrm{C} + 2\mathrm{H_2} \leftrightarrow \mathrm{CH_4}, \tag{8c}$$

$$\mathrm{R6}: \mathrm{CH_4} + \mathrm{H_2O} \leftrightarrow 3\mathrm{H_2} + \mathrm{CO}. \tag{8d}$$

Mass balance of the species i for the control volume k along the height of reaction zone can be written as

$$n_i^k = n_i^{k-1} + R_i^k \Delta V_k, \tag{9}$$

where n_i^k is the molar flow rate (mol s^{-1}), $\Delta V_k$is volume of the kth control volume (m^3), and the net rate of production of R_i^k (mol m^{-3} seconds^{-1}) is given as,

$$R_{\mathrm{H_2}}^k = r_{R4} - 2r_{R5} + 3r_{R6}, \tag{10}$$

$$R_{\mathrm{CO}}^k = 2r_{R3} + r_{R4} + r_{R6}, \tag{11}$$

$$R_{\mathrm{CO_2}}^k = -r_{R3}, \tag{12}$$

$$R_{\mathrm{CH_4}}^k = r_{R5} - r_{R6}, \tag{13}$$

$$R_{\mathrm{H_2O}}^{\mathrm{k}} = -r_{R4} - r_{R6}, \tag{14}$$

$$R_{\mathrm{C}}^k = -r_{R3} - r_{R4} - r_{R5}, \tag{15}$$

$$R_{\mathrm{N_2}}^k = 0. \tag{16}$$

The volumetric reaction rates of four chemical reactions have been given as[35]

$$r_{R3} = C_{\mathrm{RF}}A_{R3}\exp\left(\frac{-E_{R3}}{R_mT}\right)\left(y_{\mathrm{CO_2}} - \frac{y_{\mathrm{CO}}^2}{K_{R3}}\right), \tag{17a}$$

$$r_{R4} = C_{\mathrm{RF}}A_{R4}\exp\left(\frac{-E_{R4}}{R_mT}\right)\left(y_{\mathrm{H_2O}} - \frac{y_{\mathrm{H_2}}y_{\mathrm{CO}}}{K_{R4}}\right), \tag{17b}$$

$$r_{R5} = C_{\mathrm{RF}}A_{R5}\exp\left(\frac{-E_{R5}}{R_mT}\right)\left(y_{\mathrm{H_2}}^2 - \frac{y_{\mathrm{CH_4}}}{K_{R5}}\right), \tag{17c}$$

$$r_{R6} = C_{\mathrm{RF}}A_{R6}\exp\left(\frac{-E_{R6}}{R_mT}\right)\left(y_{\mathrm{H_2O}}y_{\mathrm{CH_4}} - \frac{y_{\mathrm{CO}}y_{\mathrm{H_2}}^3}{K_{R6}}\right), \tag{17d}$$

where constants of the parameters can be found in Reference 36.

The energy conservation on the kth element can be expressed as

$$\begin{aligned} &\sum_{i=1}^{6} n_i^{k-1}H_i^{k-1} + n_7^{k-1}C_{p,C}\left(T^{k-1} - T_0\right) + m_{\mathrm{ash}}C_{p,\mathrm{ash}}\left(T^{k-1} - T_0\right) \\ &= \sum_{i=1}^{6} n_i^kH_i^k + n_7^kC_{p,C}\left(T^k - T_0\right) + m_{\mathrm{ash}}C_{p,\mathrm{ash}}\left(T^k - T_0\right). \end{aligned} \tag{18}$$

2.3 | Product gas cleaning

Post cleanup of product gas is adopted to meet SOFC operation. For simple calculation, the flowrate of syngas is constant and temperature is assumed to be reduced by 50°C after leaving the hot gas cleaning unit.

$$n_4 = n_3. \tag{19}$$

The energy balance can be calculated as

$$H_4 = \sum_{i=1}^{6}[n_{4,i} \cdot h_{4,i}(T_3 - 50)]. \tag{20}$$

2.4 | Solid oxide fuel cell

The lumped model of SOFC has been developed by the authors in papers.[19,37] The input parameters for SOFC are given in Table 3.

Internal reforming reactions and the electrochemical reaction occur simultaneously due to the high operating temperature of SOFC,

$$\mathrm{CO} + \mathrm{H_2O} \leftrightarrow \mathrm{CO_2} + \mathrm{H_2},$$

$$\mathrm{CH_4} + \mathrm{H_2O} \leftrightarrow \mathrm{CO} + 3\mathrm{H_2},$$

TABLE 3 Input data for calculation of SOFC

Parameters	Value
Operating temperature	800°C
Fuel utilization, U_f	0.85
Cathode thickness, δ_c	50 μm
Electrolyte thickness, δ_e	150 μm
Anode thickness, δ_a	50 μm
Cathode resistivity, ρ_c	0.008114 exp (600/T) (Ω cm)
Electrolyte resistivity, ρ_e	0.00294 exp (10 350/T) (Ω cm)
Anode resistivity, ρ_a	0.00298 exp (−1392/T) (Ω cm)
Limiting current density, i_L	4000 A m^{-2}
Pre-exponential factor, γ_a	5.5 × 10^8 A m^{-2}
Pre-exponential factor, γ_c	7 × 10^8 A m^{-2}
$E_{act,a}$	10^5 J mol^{-1}
$E_{act,c}$	1.2 × 10^5 J mol^{-1}
Current, I	40 A
DC/AC inverter efficiency	98%

$$H_2 + \frac{1}{2}O_2 \leftrightarrow H_2O. \tag{21}$$

The equilibrium constants of shift and reforming reactions are,

$$K_R = \frac{p_{H_2}^3 p_{CO}}{p_{CH_4} p_{H_2O}} (\text{reforming}), \tag{22}$$

$$K_s = \frac{p_{H_2} p_{CO_2}}{p_{CO} p_{H_2O}} (\text{shifting}). \tag{23}$$

Furthermore, the two specific equations can be derived by

$$K_{S,SOFC} = \frac{\left(CO_2^{in} + y\right)\left(H_2^{in} + 3x + y - z\right)}{\left(CO^{in} + x - y\right)\left(H_2O^{in} - x - y + z\right)}, \tag{24}$$

$$K_R = \frac{\left(\frac{H_2^{in}+3x+y-z}{n_{tot}^{in}+2x}\right)^3 \left(\frac{CO^{in}+x-y}{n_{tot}^{in}+2x}\right)}{\left(\frac{CH_4^{in}-x}{n_{tot}^{in}+2x}\right)\left(\frac{H_2O^{in}-x-y+z}{n_{tot}^{in}+2x}\right)}, \tag{25}$$

where x and y are the flow rates of CH_4 and CO taking part in the two reactions, while the reaction rate z is calculated by the Faraday's Law.

$$z = I/(2F). \tag{26}$$

Therefore, the output voltage is calculated by

$$V = E_0 - \eta_{act,a} - \eta_{act,c} - \eta_{ohm} - \eta_{con}, \tag{27}$$

where η_{act}, η_{ohm}, and η_{ohm} are three kinds of polarizations, respectively.

The open circuit voltage E_0 is calculated by the Nernst equation

$$E_0 = \frac{-\Delta G_0}{2F} + \frac{RT}{2F} \ln \frac{p_{H_2} \cdot \left(p_{O_2}\right)^{1/2}}{p_{H_2O}}. \tag{28}$$

The detailed electrochemical model of SOFC is available in References 38,39.

The energy balance equation is

$$\sum_i H_i^{in} + \sum_k R_k(-\Delta H_k) = W_{SOFC} + \sum_i H_i^{out}, \tag{29}$$

where the output electrical power of SOFC is given by

$$W_{SOFC} = IV. \tag{30}$$

2.5 | Combustor, gas turbine, and compressor

In this work enough air is supplied from the exit of SOFC cathode, SOFC, H_2, CO, and CH_4 can be consumed completely in the combustor.

The adiabatic combustion temperature can be derived from energy balance about the combustor

$$\sum_{i=1}^{7} n_i^{in} \left(\Delta H_f^0 + \int_{298}^{T_{in}} C_p dT\right) = \sum_{i=1}^{4} n_i^{out} \left(\Delta H_f^0 + \int_{298}^{T_{out}} C_p dT\right). \tag{31}$$

The outlet temperatures and work of the compressor and gas turbine are given below[40]:

$$\frac{T_{COM,out}}{T_{COM,in}} = \frac{T_{GT,in}}{T_{GT,out}} = \pi^{\frac{k-1}{k}}, \tag{32}$$

$$W_{COM} = \frac{1}{\eta_{COM,s}} [H(T_{COM,out}) - H(T_{COM,out})], \tag{33}$$

$$W_{GT} = \eta_{GT,s} [H(T_{GT,in}) - H(T_{GT,out})], \tag{34}$$

where π is the pressure ratio and η_s is the isentropic efficiency.

2.6 | LiBr–H_2O absorption chiller

Exhausted gases from the gas turbine can be further utilized to improve the cooling capacity to recover waste heat. The single effect LiBr–H_2O absorption refrigeration system (ARS) is chosen in this work.[41] The main components of the ARS are a generator, evaporator, condenser, absorber, and solution heat exchanger (SHX) as shown in Figure 1. The absorbent is LiBr and the refrigerant is water.

The following assumptions are made to evaluate the cooling capacity.

1. The temperature variations and mass accumulation in the condenser, generator, absorber, evaporator, and the solution heat exchanger are not considered.
2. The pressure drop in components is neglected, and the expansion process of expansion devices is adiabatic.
3. The heat loss of the generator and gains of the evaporator from the surroundings are neglected.
4. The refrigerant at the outlet of generator is superheated and saturated liquid at the outlet of the condenser and saturated vapor at the outlet of the evaporator.

Mass and energy balances of the generator:

$$m_{23} = m_{24} + m_{27}, \tag{35}$$

$$Q_g = m_{24}h_{24} + m_{27}h_{27} - m_{23}h_{23}. \tag{36}$$

For condenser:

$$m_{27} = m_{28}, \tag{37}$$

$$Q_c = m_{27}h_{27} - m_{28}h_{28}. \tag{38}$$

For evaporator:

$$m_{29} = m_{30}, \tag{39}$$

$$Q_e = m_{30}h_{30} - m_{29}h_{29}. \tag{40}$$

For absorber:

$$m_{21} = m_{26} + m_{30}, \tag{41}$$

$$Q_a = m_{26}h_{26} + m_{30}h_{30} - m_{21}h_{21}. \tag{42}$$

The solution heat exchanger

$$m_{23}X_{23} = m_{24}X_{24}, \tag{43}$$

$$X_{21} = X_{22} = X_{23}, \tag{44}$$

$$X_{24} = X_{25} = X_{26}. \tag{45}$$

X is the concentration of LiBr in the solution (%, $kg\,kg^{-1}$).

Heat exchanger effectiveness is defined as

$$\varepsilon = \frac{T_{24} - T_{25}}{T_{24} - T_{22}}, \tag{46}$$

$$m_{24}(h_{24} - h_{25}) = m_{22}(h_{23} - h_{22}). \tag{47}$$

The coefficient of performance (COP) of absorption chiller is defined by

$$\mathrm{COP} = \frac{Q_e}{Q_g}. \tag{48}$$

2.7 | Cooling, heating, and net power output

The cooling load ($Q_{cooling}$) is equal to the heat transfer rate Q_e in the evaporator

$$Q_{cooling} = Q_e. \tag{49}$$

The available heat from gases out of the generator can be further recovered by a heat exchanger to generate domestic hot water. The heating load is defined as the output heating of heat exchanger in which the inlet feed water is assumed as 25°C and outlet domestic hot water is 60°C.

$$Q_{heating} = n_{16}(h_{18} - h_{16}). \tag{50}$$

Net power output of the CCHP system is expressed as:

$$W_{net} = W_{GT} + W_{SOFC} - W_{Compressor\text{-}1} - W_{Compressor\text{-}2} - W_{Pump}. \tag{51}$$

The electrical efficiency and CCHP efficiency are given as

$$\eta_{el} = \frac{W_{net}}{\dot{m}_{biomass}\mathrm{LHV}_{biomass}}, \tag{52}$$

$$\eta_{CCHP} = \frac{Q_{cooling} + Q_{heating} + W_{net}}{\dot{m}_{biomass}\mathrm{LHV}_{biomass}}. \tag{53}$$

2.8 | Exergy analysis

With the second law of thermodynamics, exergy analysis is used to investigate the irreversibilities in components and the whole performance of CCHP.[42]

The general exergy rate balance can be written:

$$\left(1-\frac{T_0}{T}\right)\dot{Q}_{\mathrm{i}}+\sum_{\mathrm{i}}\dot{m}_i ex_i-\sum\dot{m}_e ex_e-\dot{W}-\dot{Ex}_{\mathrm{D}}=0. \quad (54)$$

Where the first term is the heat of exergy. The second terms are the sum of exergy input and output rates of the flow, respectively. The third term is the work leaving the system. The last term is the exergy destruction rate.

The specific flow exergy is expressed by the sum of specific physical and chemical exergy.

$$\mathrm{ex}=\mathrm{ex}^{\mathrm{ph}}+\mathrm{ex}^{\mathrm{ch}}. \quad (55)$$

The physical exergy can be defined as

$$\mathrm{ex}^{\mathrm{ph}}=h-h_0-T_0(s-s_0). \quad (56)$$

The chemical exergy for an ideal gas mixture can be written as

$$\mathrm{ex}^{\mathrm{ch}}=\sum_i x_i\left(\mathrm{ex}_i^{ch}+RT_0\ln x_i\right), \quad (57)$$

where x_i is the molar fraction, $\mathrm{ex}_i^{\mathrm{ch}}$ the standard chemical exergy of species i which can be taken from Reference 43.

The exergy destruction ratio of each component is defined as the ratio of exergy destruction to total exergy input. It can be written as

$$\eta_{\mathrm{Ex},i}=\frac{\mathrm{Ex}_{\mathrm{dest},i}}{\dot{m}_{\mathrm{biomass}}\mathrm{Ex}_{\mathrm{bio}}^{\mathrm{ch}}}. \quad (58)$$

Consequently, the exergetic efficiency for the entire CCHP system can be defined as follows:

$$\eta_{\mathrm{CCHP,ex}}=\frac{Q_{\mathrm{cooling}}\left(1-\frac{T_0}{T_{\mathrm{cool}}}\right)+Q_{\mathrm{heating}}\left(1-\frac{T_0}{T_{\mathrm{heat}}}\right)+W_{\mathrm{net}}}{\dot{m}_{\mathrm{biomass}}\mathrm{Ex}_{\mathrm{bio}}^{\mathrm{ch}}}. \quad (59)$$

At the assumed condition of environment, the physical exergy of biomass is zero and the chemical exergy of biomass can be expressed as

$$\mathrm{Ex}_{\mathrm{bio}}^{\mathrm{ch}}=\beta\mathrm{LHV}_{\mathrm{bio}}, \quad (60)$$

where the factor is given by Reference 43.

$$\beta=\frac{1.044+0.00160\cdot\mathrm{H/C}-0.3493\cdot\mathrm{O/C}(1+0.0531\cdot\mathrm{H/C})+0.0493\mathrm{N/C}}{1-0.4124\mathrm{O/C}}. \quad (61)$$

2.9 | Economic analysis

In this work, the net present value (NPV) method[44] is used to analyze the economic performance of this CCHP system. NPV is expressed as follows

$$\mathrm{NPV}=\sum_{k=0}^{n}\frac{C_k}{(1+r)^k}=-C_0+\sum_{k=1}^{n}\frac{C_k}{(1+r)^k}. \quad (62)$$

The initial cost of investment of the whole CCHP system C_0 (€) is given by

$$C_0=C_{\mathrm{gasfier}}+C_{\mathrm{MGT}}+C_{\mathrm{SOFC}}+C_{\mathrm{clean}}+C_{\mathrm{ARS}}+C_{\mathrm{HRU}}, \quad (63)$$

which is the sum of components cost in the CCHP such as a gasifier, SOFC, GT, ARS, and HRU.

The term C_k is shown in Equation (54)

$$C_k=C_{\mathrm{ele}}+C_{\mathrm{cool}}+C_{\mathrm{heat}}-(C_{\mathrm{fuel}}+C_{\mathrm{MGT,OM}}+C_{\mathrm{SOFC,OM}}+C_{\mathrm{clean,OM}}), \quad (64)$$

where C_{ele}, C_{cool}, and C_{heat} are yearly revenues of electricity, cool and heat energy, respectively, €/year, C_{fuel} is fuel cost, $C_{\mathrm{SOFC,OM}}$, $C_{\mathrm{MGT,OM}}$, and $C_{\mathrm{clean,OM}}$ are the O&M costs of SOFC, MGT, and gas cleaning unit respectively, €/year.

Accordingly, as NPV equals to zero, the internal rate of return (IRR) and payback period (PB) can be determined by

$$\mathrm{NPV}=\sum_{k=0}^{n}\frac{C_k}{(1+\mathrm{IRR})^k}=0, \quad (65)$$

and

$$\mathrm{NPV}=\sum_{k=0}^{\mathrm{PB}}\frac{C_k}{(1+r)^k}=0. \quad (66)$$

3 | RESULTS AND DISCUSSION

The models of single-effect LiBr–H_2O ARS and downdraft gasifier have been verified against experimental or simulation results available in other literatures.[27,34]

TABLE 4 Comparison between this work and references

Gas Composition (%)	This Work	Reference 34		This Work	Reference 27
CO	21.83	19.6	Q_g (kW)	259.45	246.21
H_2	20.30	17.2	Q_c (kW)	213.56	206.15
CO_2	8.26	9.9	Q_a (kW)	247.47	241.34
CH_4	1.0	1,4	Q_e (kW)	201.29	201.29
N_2	48.61	51,9	COP	0.7758	0.8175

It is seen from Table 4 that models of this work are in good agreement with the experimental or simulation results of References 27,34.

The simulation of the CCHP system begins from the one-dimensional model of the downdraft gasifier. The syngas compositions (state 3) are determined by Equations (4)-(17) using the Newton-Raphson method. The syngas temperature is obtained by energy Equation (18) using the bisection method. These data are transferred as input data to the entrance of the SOFC. The electrochemical model of SOFC determines terminal voltage and electric power. The energy balance Equation (29) accepts these results and gives the molar flow rate of air at the cathode inlet. The air flow rate entering the cathode is applied to the electrochemical model for the next calculation of cell terminal voltage and power until the convergence is obtained.

The gas temperature and mass of the combustor exit are not known at the beginning of the simulation; in order to run the whole system model, a set of initial parameters have to be assumed for the calculation of heat exchanger, ARS, and other components until convergence is met eventually. Once thermodynamic properties of all state points of CCHP are provided, the energy and exergy analysis can be conducted.

A set of operating parameters and the assumed efficiencies of the system components are given in Table 5.

Based on the thermodynamic models of these components, the impact of main operating parameters on the energetic and economic performance of CCHP system is investigated.

TABLE 5 Input data and designed performance of components for the baseline case

Parameters	Value
Biomass	
Moisture content (state 1)	40%
Mass flow rate of biomass (state 1)	28.33 kg h^{-1}
Gasifier	
Moisture content of biomass (state 2)	15%-35%
Molar fraction of air	21% O_2, 79% N_2
Mass flow rate of air (MA = 100%)	46.99 kg h^{-1}
Gasifier dimension	[34]
Compressor and gas turbine	
Isentropic efficiency of compressor	0.8
Pressure ratio of compressor	2.5
Isentropic efficiency of gas turbine	0.85
Outlet temperature of GT (state 11)	770°C
Heat recover unite (HRU)	
Inlet temperature of water (state 16)	25°C
Temperature of domestic hot water (state 18)	60°C
Absorption refrigerator system (ARS)	
Working pairs	LiBr–H_2O
High pressure	7300 Pa
Low pressure	991.75 Pa
Solution heat transfer effectiveness	0.64
Exhaust temperature (state 15)	130°C

3.1 | Mass flowrate of air (MA) in a gasifier

Mass flowrate plays a crucial role on CCHP energetic and exergy efficiency since it has a decisive impact on the syngas composition. Table 6 gives mass flowrate, temperature, pressure, and stream composition at different state points for baseline case.

The effect of MA on the syngas composition, the powers of compressors, gas turbine, SOFC, and the net power of the whole CCHP system are shown in Figures 2 and 3, respectively. Exergy destruction ratio of some components is shown in Figure 4. Exergy destruction ratios for other components (eg, dryer, gas cleaner, SOFC, gas turbine, compressor-1, and pump) are relatively smaller and not presented separately. The effect of MA on the heating, cooling, electrical efficiency, and whole CCHP energy and exergy efficiencies is shown in Figures 5 and 6.

TABLE 6 The thermodynamic properties of different state points for baseline case

State	m (kg s^{-1})	T (K)	p (atm)	Gas Composition (% vol)						
				CO	CO_2	H_2	H_2O	CH_4	N_2	O_2
1	0.0078	298	1	–	–	–	–	–	–	–
2	0.0055	298	1	–	–	–	–	–	–	–
3	0.0185	1344	2.5	17.56	11.24	18.17	6.54	0	46.40	0
4	0.0185	1295	2.5	17.56	11.24	18.17	6.54	0	46.40	0
5	0.0219	1123	2.5	5.63	23.26	4.53	20.18	0	46.39	0
6	0.226	298	1	0	0	0	0	0	79	21
7	0.226	408	2.5	0	0	0	0	0	79	21
8	0.226	1023	2.5	0	0	0	0	0	79	21
9	0.2226	1123	2.5	0	0	0	0	0	81	19
10	0.2445	1175	2.5	0	2.62	0	2.24	0	77.32	17.82
11	0.2445	1042	1.425	0	2.62	0	2.24	0	77.32	17.82
12	0.2445	489	1.425	0	2.62	0	2.24	0	77.32	17.82
13	0.2445	445	1.425	0	2.62	0	2.24	0	77.32	17.82
14	0.2445	426	1.425	0	2.62	0	2.24	0	77.32	17.82
15	0.2445	403	1.425	0	2.62	0	2.24	0	77.32	17.82
16	0.033	298	1	–	–	–	–	–	–	–
17	0.033	298	1	–	–	–	–	–	–	–
18	0.033	333	1	–	–	–	–	–	–	–
19	0.013	298	1	0	0	0	0	0	79	21
20	0.013	408	2.5	0	0	0	0	0	79	21

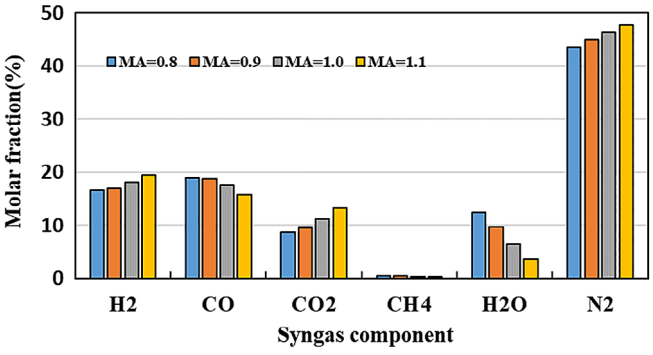

FIGURE 2 Effects of MA on syngas composition [Colour figure can be viewed at wileyonlinelibrary.com]

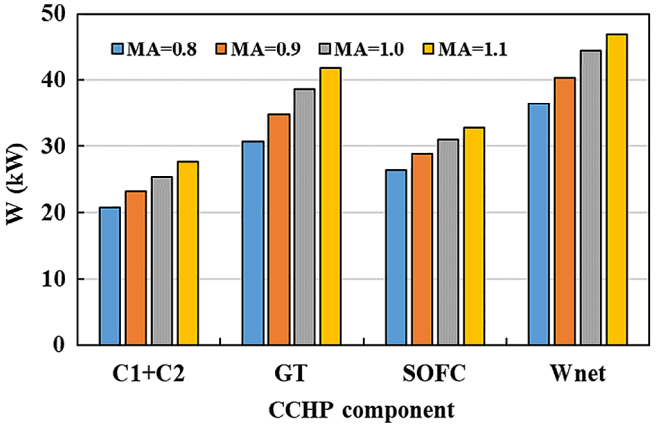

FIGURE 3 Effects of MA on power of components [Colour figure can be viewed at wileyonlinelibrary.com]

It shows that more H_2, CO_2, and N_2 yield as more air entering the gasifier. N_2 does not take part in the chemical reactions fed to the syngas. While more O_2 leads to higher reaction temperature which benefits the endothermic char conversion of R2 and R4, the concentrations of H_2 and CO_2 go up, and accordingly, the H_2O concentration decreases. However, if the gasification temperature is too high, the oxidation reaction plays more important part than the reduction reactions and the consuming of CO will overweigh the production of CO.

The largest exergy destruction lies in the gasifier since biomass is decomposed with irreversibility through chemical reactions. More air is favorable for H_2 yield and conversion of char to CO which results in a significant increase of chemical exergy at the gasifier outlet.

Therefore, the exergy destruction in a gasifier, which equals to the difference between the inlet and outlet exergy, decreases dramatically from 30% to 8% as MA increasing.

The higher MA also causes the higher ratio of H_2 to H_2O at the inlet of anode which is in favor of the output power of SOFC (Equation 28). In order to maintain the allowable operation temperature of SOFC, more air has to be introduced which results in the increase of compression work of compressor-2 and also the combustor temperature, thus improving the output work of gas turbine.

Therefore, the 8%-10% exergy destruction ratio in the combustor resulting from mixing loss and irreversible combustion process occurs. The main reason of exergy destruction in the air preheater is due to the large flowrate to maintain SOFC temperature under maximum allowable temperature, and great temperature difference between the hot and cold side of the air preheater. The exergy destruction ratio for air preheater is 5%-6%.

Since the increase trend of work output of SOFC and GT overweighs that of the work input to drive the compressors, the network of the whole system ascends with higher MA. The electricity efficiency is above 43% as MA = 0.8 and climbs to 55% as MA = 1.1.

As for the cooling and heating of CCHP, both of them increase with higher MA, while the sum of the exergy destructions rates of components decreases. The whole CCHP efficiency increases from 56% to 74% and CCHP exergy efficiency from 39% to 55% as MA varying between 0.8 and 1.1 as shown in Figure 6. The more air flows into the system, the more chemical energy of biomass is converted into power, cooling, and heating.

3.2 | Effect of biomass moisture content

Moisture content (MC) should not be too high before entering the gasifier, otherwise gasification is not technologically viable, and the entire system is unstable. In this work, the initial of MC is 0.4, and it drops to 0.15-0.35 (state 2) after drying.

Effect of MC at the inlet of the gasifier (state 2) on the syngas composition and powers of CCHP components have been shown in Figures 7 and 8. Exergy destruction ratio of some components in is shown in Figure 9.

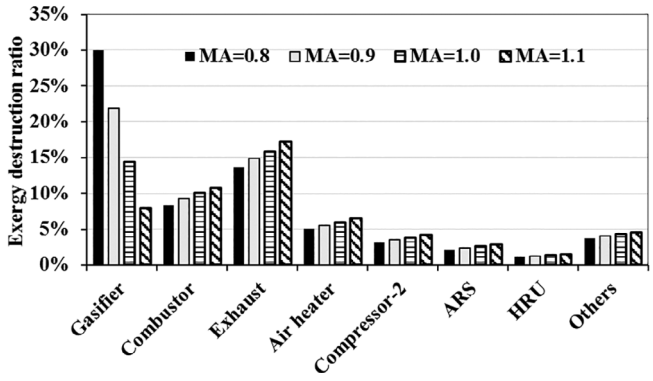

FIGURE 4 Exergy destruction ratios of components for different MA

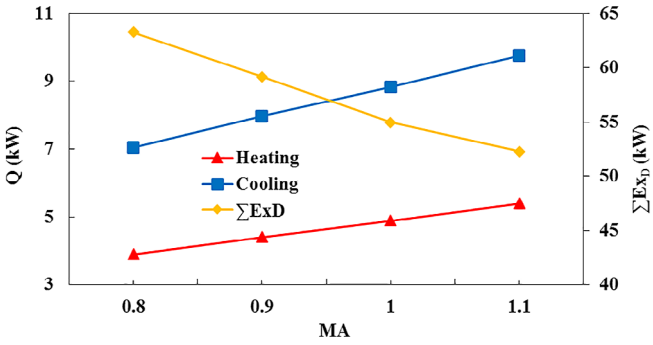

FIGURE 5 Effects of MA on cooling, heating, and total exergy destruction rate [Colour figure can be viewed at wileyonlinelibrary.com]

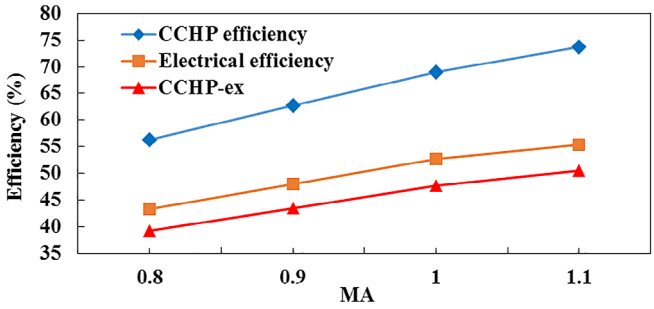

FIGURE 6 Effects of MA on electrical and CCHP energy and exergy efficiencies [Colour figure can be viewed at wileyonlinelibrary.com]

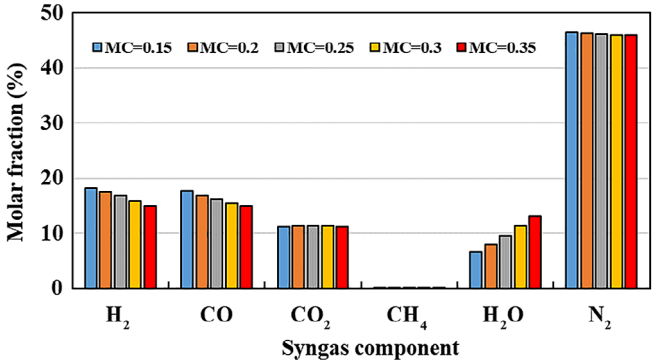

FIGURE 7 Effects of MC on syngas composition [Colour figure can be viewed at wileyonlinelibrary.com]

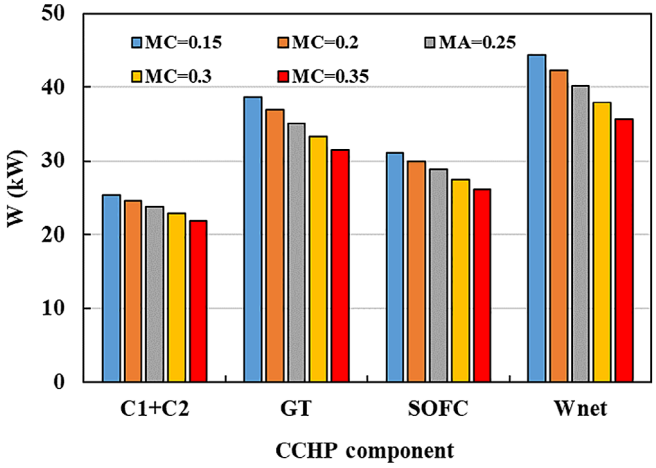

FIGURE 8 Effects of MC on power of components [Colour figure can be viewed at wileyonlinelibrary.com]

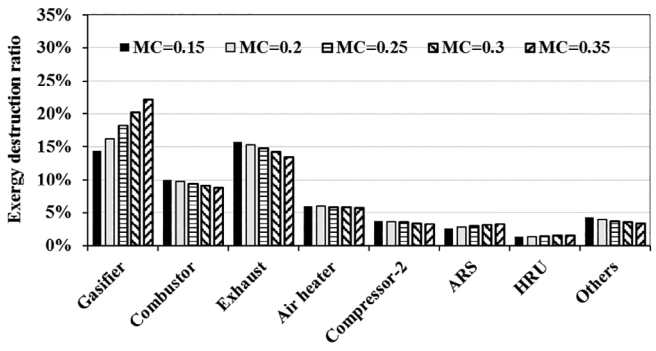

FIGURE 9 Exergy destruction ratios of components for different MC

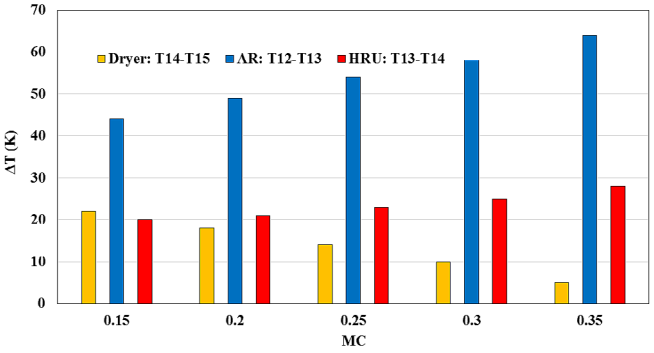

FIGURE 10 Effects of MC on temperature differences of AR, HRU, and dryer [Colour figure can be viewed at wileyonlinelibrary.com]

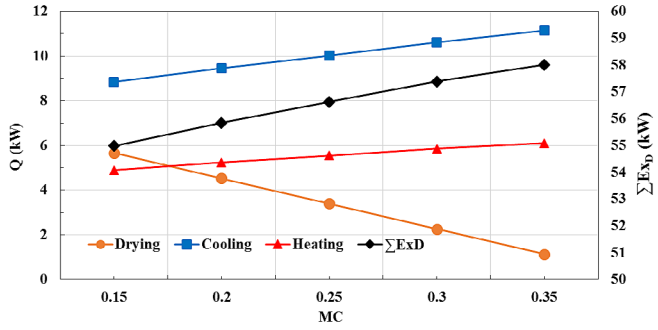

FIGURE 11 Effects of MC on cooling, heating, and total exergy destruction rate [Colour figure can be viewed at wileyonlinelibrary.com]

The composition of H_2O increases obviously, meanwhile that of H_2 and CO descend mildly and other compositions of N_2, CO_2, and CH_4 are nearly invariable. The reason is that more water in the gasifier reduces the gasification temperature, thus increasing the molar fraction of H_2O. Although more H_2O improves the methane–water–gas reaction (R4) and reforming reaction (R6), the increase trend of CO production is offset completely due to the lower temperature which is unfavorable for the release of CO from the reduction reactions. In the same way, the yield of H_2 is controlled mainly by the temperature rather than the composition of gas mixture. Accordingly, the exergy destruction ratio of the gasifier climbs from 14% to 22% which is the main exergy destruction of the CCHP system. The exergy destruction ratios of other components change slightly with different MC.

The temperature differences of exhaust gas passing through the absorption refrigerator, HRU, and dryer are shown in Figure 10. Figure 8 gives powers of compressors, SOFCs, and gas turbine at a specific value of MC. As analyzed above, a lower ratio of H_2 to H_2O determines the less output work of SOFC; meanwhile, the lower combustor temperature due to more steam flowing into the combustor from the anode outlet reduces the output work of gas turbine. Although compression work of compressors decreases moderately because of MC, the drop of output power of SOFC and GT is more obvious, and, hence, the network of the whole system falls from 44 kW to 35 kW as MC varying from 0.15 to 0.35.

The lower MC at the inlet of gasifier means higher drying degree which results from larger temperature difference of hot exhaust passing dryer; it means that more energy is provided to heat the moisture and superheat the vapor. Accordingly, both of temperature differences pass through AR and HRU go up as MC rising. It also results in the increase of exergy destruction ratio of ARS and HRU.

Accordingly, impact of MC on drying, cooling, and heating energy and total exergy destruction rate of CCHP system are shown in Figure 11. In this work, the heat for drying goes down remarkably from 5.6 to 1.1 kW, while the value of heating climbs from 4.8 to 6.1 kW, cooling

from 8.8 to 11 kW, and the total exergy destruction rate of CCHP from 55 to 58 kW as MC increases from 0.15 to 0.35.

Effect of MC on the electrical efficiency and CCHP efficiency is shown in Figure 12. Higher MC has a notable negative impact on the net output work as discussed above; therefore, the electrical efficiency and CCHP decrease. Meanwhile, higher MC at the entrance of the gasifier shows less heat to evaporate water in the dryer, thus, more chemical energy of biomass could be converted into heating and cooling. In this work, only if MC < 0.3, the electrical efficiency is above 45% and the CCHP efficiency larger than 65% and exergy efficiency up to 40% can be reached.

3.3 | Effect of temperatures of generator (Tg) and absorber (Ta)

In this study, the higher pressure of condensation and lower pressure of the evaporator is kept constant as shown in Table 5. The effects of Tg (state 24) and Ta (state 21) on the cooling capacity, COP, and CCHP efficiency can be obtained by varying them respectively while holding all the other input constants at the baseline values listed in Table 5.

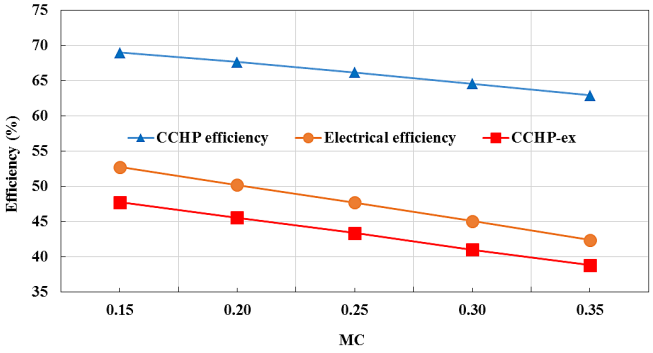

FIGURE 12 Effects of MC on electrical and CCHP energy and exergy efficiencies [Colour figure can be viewed at wileyonlinelibrary.com]

The thermodynamic properties of each state-point of AR is shown in Table 7, and summary of energy quantities is provided in Table 8 as Tg = 85°C and Ta = 35°C.

It can be seen that the liquid flowrate of weak solution through the solution pump is about 10 times that of the refrigerant, leaving the generator. The COP of ARS is 77.52%.

Applying the exergy rate balance equation to each component of the ARS, the component exergy destruction rates can be calculated, as shown in Figure 13. It is clear that the evaporator and absorber account for the highest exergy destruction rates compared with other components. In the evaporator, phase change with high temperature differences between the working fluids and the refrigerated space results in a significant entropy creation rate. The absorber occupied the second largest exergy destruction rate of ARS because of the large heat transfer temperature differences. Total exergy destruction rate of ARS grows from 2.312 to 2.742 kW as Tg from 80°C to 95°C.

The effect of varying of Tg and Ta on the cooling capacity (Q_e) and COP is shown as Figures 14 and 15, respectively. The lower the Ta and the higher the Tg, the better the cooling capacity and COP. In this study, the cooling capacity and COP gain the maximum of 9.468 kW and 83% as Tg = 95°C and Ta = 25°C. As Tg falling to 80°C and Ta rising to 40°C they seriously deteriorate to 5.555 kW and 49%. Accordingly, CCHP drops by 5% from 70% to 65% as shown in Figure 16.

The decay rate of cooling and COP slow down at higher Tg due to higher Ta. For the same increase extent of Ta from 25°C to 40°C, the COP descends by 6% as Tg = 95°C, while it declines by 34% as Tg = 80°C.

TABLE 7 The thermodynamic properties of single LiBr–H_2O absorption chiller

State	Substance	T (°C)	P (Pa)	m (kg s^{-1})	X (%)	h (J kg^{-1})	S (J kg^{-1} K^{-1})
21	LiBr–water	35	991.75	0.0372	53.88	110 220	230
22	LiBr–water	35	7300	0.0372	53.88	110 220	230
23	LiBr–water	67	7300	0.0372	53.88	176 430	434
24	LiBr–water	85	7300	0.0335	59.95	237 740	485
25	LiBr–water	46	7300	0.0335	59.95	164 090	269
26	LiBr–water	46	991.75	0.0335	59.95	164 090	269
27	Water vapor	85	7300	0.0037	0	2 659 800	8509
28	Water	40	7300	0.0037	0	167 472	620
29	Water	7	991.75	0.0037	0	167 472	627
30	Water vapor	7	991.75	0.0037	0	2 514 800	8995

TABLE 8 Summary of energy quantities

	Variable	Unit	Value
Q_a	Absorber heat transfer rate	kW	10.859
Q_c	Condense heat transfer rate	kW	9.386
Q_e	Evaporator heat transfer rate	kW	8.841
Q_g	Generator heat transfer rate	kW	11.405
Q_{she}	Solution heat exchanger heat transfer rate	kW	2.465
$\sum Ex_D$	Total exergy loss of the ARS	kW	2.472
COP	Coefficient of performance	%	77.52

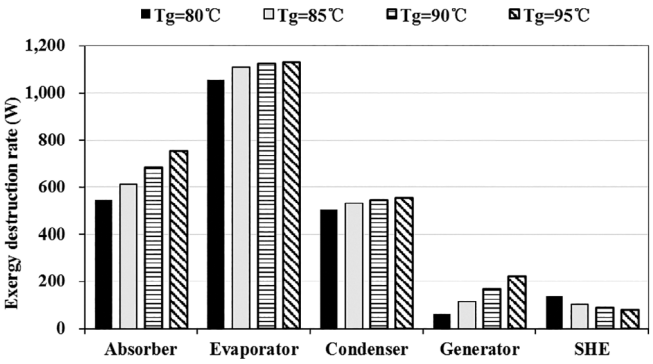

FIGURE 13 Exergy destruction rates of components of the ARS (Ta = 35°C)

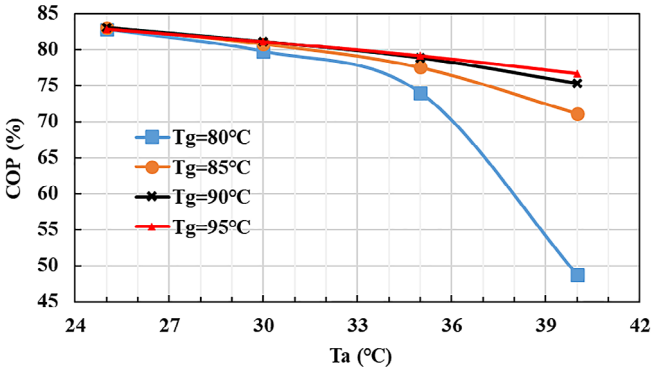

FIGURE 15 Effects of Tg and Ta on COP [Colour figure can be viewed at wileyonlinelibrary.com]

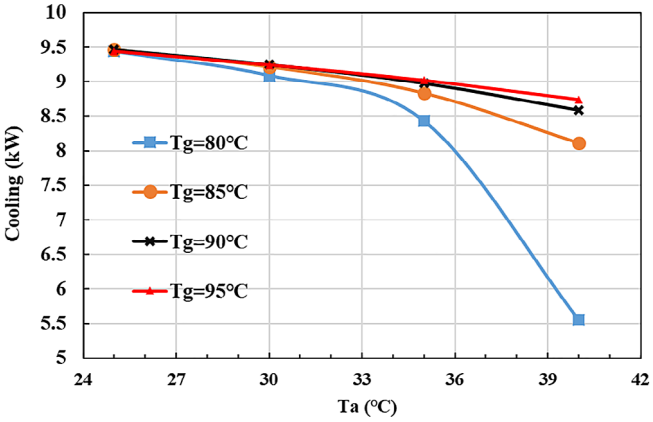

FIGURE 14 Effects of Tg and Ta on cooling energy [Colour figure can be viewed at wileyonlinelibrary.com]

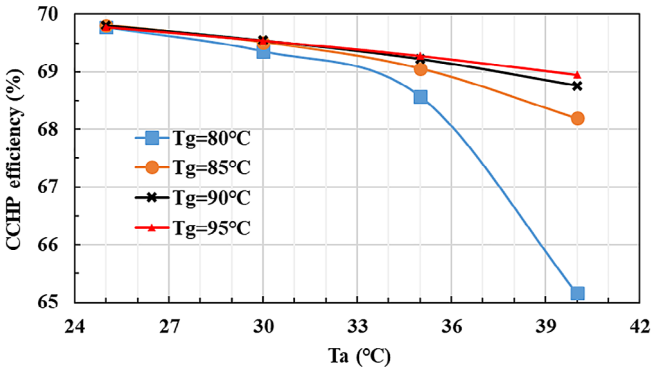

FIGURE 16 Effects of Tg and Ta on CCHP efficiency [Colour figure can be viewed at wileyonlinelibrary.com]

3.4 | Effect of exhaust gas temperature

Due to exhaust's high temperature and mass flow rate, it has a high-energy flow rate. This part of heat energy coming from the biomass chemical energy is wasted. The baseline value of exhaust gas (state 15) is assumed as 130°C. In this work, it shows that exhaust ranks the third (above 10%) among all exergy destruction ratios of the component. In order to improve the efficiency, this temperature could be decreased further.

Figure 17 gives the temperature differences in the AR and HRU to generate the cooling and heating energy. It shows that the temperature difference grows gradually with the lower temperature of exhaust gas. Accordingly, the values of heating and cooling energy go up as shown in Figure 18.

Reducing the exhaust temperature from 130°C to 90°C increases the values of cooling energy from 8.84 to 14.3 kW

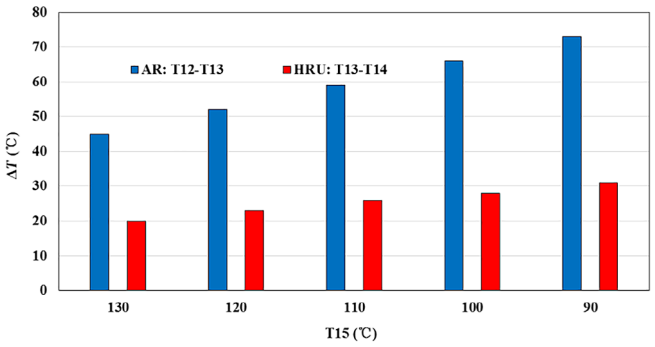

FIGURE 17 Effects of exhaust temperature on temperature differences of AR and HRU [Colour figure can be viewed at wileyonlinelibrary.com]

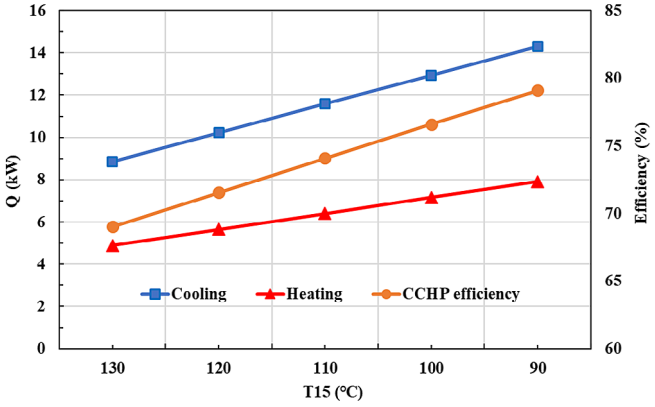

FIGURE 18 Effects of exhaust temperature on CCHP cooling, heating, and efficiency [Colour figure can be viewed at wileyonlinelibrary.com]

and subsequently, the heating energy from 4.8 to 8 kW. The exergy rate of exhaust (state 15) drops from 13.33 to 11.11 kW. Although the exhaust has a high-energy flowrate due to its high temperature and mass flow rate, the exhaust cannot be utilized for useful work or heat because the exhaust temperature has to be above the dew point to prevent the condensation of fuel gas in chimney.

Since more chemical energy of biomass converts to heating and cooling as the temperature of exhaust gas drops from 130°C to 90°C, the total CCHP efficiency increases by 10% and reaches 79%.

3.5 | Economic analysis

Based on the thermodynamic analysis, the economic study of CCHP system is carried out. The input data for the economic study are presented in Table 9, and the other data are kept at constant as shown in Table 5. The corresponding economical result is shown in Table 10.

TABLE 9 Input data for the economic analysis of CCHP[22,33,45-50]

Parameter	Unit	Value
Annual working time	hour	7000
Life time	year	10
Discount rate, *r*	%	7
Gasifier	€	12 600
SOFC capital investment	€/kW	4250
SOFC O&M	€/kW-y	54
Clean unit initial capital investment	€/kW	459
Clean unit O&M	€/kW-y	57
MGT capital investment	€/kW	2820
MGT O&M	€/kW-y	124
Absorption chiller	€/kW	300
HRU	€	3000
Wood price	€/kg	0.112
Electricity price	€/kWh	0.236
Heating price	€/kWh	0.075
Cooling price	€/kWh	0.067

TABLE 10 The economic analysis results of CCHP

Parameters	Unit	Value
C_{SOFC}/C_0	%	46.76
Yearly O&M cost	k€	31.81
Yearly electrical income	k€	73.35
Yearly cooling income	k€	4.15
Yearly heating income	k€	2.57
Yearly total income	k€	48.26
Net present value (NPV)	k€	86.79
Internal rate of return (IRR)	%	16.63
Payback period (PB)	Years	6.91

Investment cost of SOFC is almost half of the total investment of CCHP. In this work, the NPV values becomes positive from the 7th year since the PB is equal to 6.91 years, and it reaches 86.79 k€ at the end of 10th year as shown in Table 10. This confirms that the CCHP system has economic potential.

In spite of the SOFC's high electrical efficiency, it is obvious that the capital cost of SOFC occupies the maximum proportion of the whole investment of CCHP, which is a decisive factor for the CCHP containing SOFC competing with other CCHP system. Therefore, more attention should be paid on the impact of SOFC on the overall economic performance of CCHP.

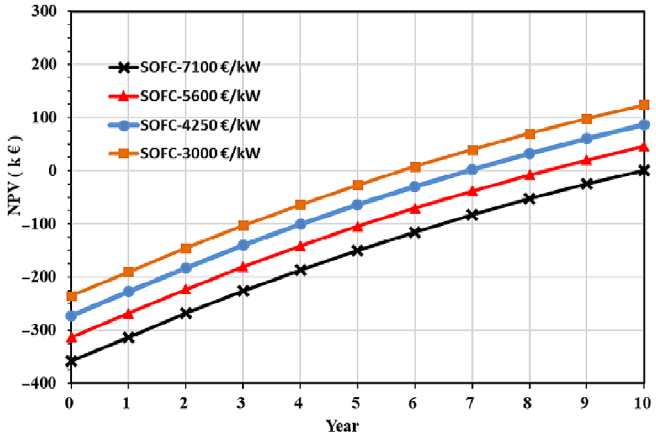

FIGURE 19 Effect of SOFC investment costs on NPVs of CCHP [Colour figure can be viewed at wileyonlinelibrary.com]

TABLE 11 Effect of SOFC cost on the economic performance of CCHP

Parameters	Unit	Value			
SOFC initial cost	€/kW	7100	5600	4250	3000
C_{SOFC}/C_0	%	59.47	53.64	46.76	38.27
Net present value (NPV)	k€	1.29	46.29	86.79	124.29
Payback period (PB)	Years	9.97	8.26	6.91	5.77

The impacts of SOFC costs on the NPV have been given in Figure 19. The economic results for the different SOFC initial costs are shown in Table 11.

It is clear that the NPV increases with the lower price of SOFC. The NPV booms from 1.29 to 124.29 k€ as the SOFC cost drops from 7100 to 3000 €/kW in the future, accordingly PB declines from 9.97 to 5.77 years. In this work, 7100 €/kW is the acceptable highest cost of SOFC investment, since its PB is almost the system lifetime.

Nowadays, the SOFC costs are still more than half of the total investment for some CCHP systems,[12] which hinders the commercialization of the CCHP based on SOFC as a prime mover. If the costs below 3000€/kW could be achieved in future, the proportion of SOFC cost will be less than 40% as show in Table 11. Thus, the CCHP system including SOFC will be more competitive compared with other CCHP systems.

4 | CONCLUSIONS

In this work, a novel biomass-based CCHP system composed of a downdraft gasifier, SOFC, micro GT, and absorption chiller is investigated. Impacts of some important operating parameters on the energetic, exergy, and economic performance of CCHP are explored in detailed.

The results of this work could be listed as follow.

- Mass flowrate of air for gasification plays a crucial role on improving the overall CCHP efficiencies since the gasifier accounts for the largest proportion (up to 30%) in total exergy destruction rate. Adjusting MA can increase exergy efficiency by 10%.
- Reducing the moisture content (MC) of biomass is an effective way for the improvement of the output of cooling, heating, and power in system. Smaller value of MC(<0.2) could results in exergy efficiency greater than 45% and CCHP efficiency over 65%.
- The decrease of exhaust gas temperature boots the production of cooling and heating of the CCHP system. A 10% improvement of overall efficiency of CCHP can be obtained as the exhaust gas temperature decreases from 130°C to 90°C.
- Higher temperature of generator leads to promotion of cooling production and COP of absorption chiller. In this work, the variation range of generator temperature between 85°C and 95°C could obtain COP larger than 0.7 and avoid crystallization of LiBr–H_2O solution.
- The SOFC initial investment plays the main part in the economically feasibility of this CCHP. Once the cost of SOFC is below about 3000€/kW in future, the CCHP including SOFC as a prime mover will be more competitive with other CCHP system.
- In general, for the baseline case in this work, CCHP can achieve an electrical efficiency of 52%, exergy efficiency of 47%, CCHP efficiency of 70% and payback period of 7 years.

To overcome the shortcomings of this study, some works will be carried out for future research

- A heat transfer model will be added to ARS which allows for a more realistic set of inputs to a simulation model, and it will be helpful to gain more complete understanding of ARS irreversibilities in a practical machine.
- Life cycle assessment and environmental analysis would be adopted to estimate the greenhouse gas reductions and environmental impacts of this CCHP.
- Multiobjective optimization will be used for this CCHP to find the best strategies about trade-off among the efficiency improvement, energy saving, and greenhouse gas reductions.

ACKNOWLEDGEMENT

The first author is grateful for the financial support from China Scholarship Council (CSC).

ORCID

Junxi Jia https://orcid.org/0000-0002-8818-6975

REFERENCES

1. Dincer I, Acar C. A review on clean energy solutions for better sustainability. *Int J Energy Res*. 2015;39:585-606.
2. Pan S-Y, Du MA, Huang I-T, Liu I-H, Chang E-E, Chiang P-C. Strategies on implementation of waste-to-energy (WTE) supply chain for circular economy system: a review. *J Clean Prod*. 2015;108:409-421.
3. Stryi-hipp G. Introduction to renewable heating and cooling. *Renewable Heating and Cooling*. Cambridge: Woodhead Publishing; 2016.
4. Mehrpooya M, Sayyad S, Zonouz MJ. Energy, exergy and sensitivity analyses of a hybrid combined cooling, heating and power (CCHP) plant with molten carbonate fuel cell (MCFC) and Stirling engine. *J Clean Prod*. 2017;148:283-294.
5. Wegener M, Malmquist A, Isalgué A, Martin A. Biomass-fired combined cooling, heating and power for small scale applications – a review. *Renew Sustain Energy Rev*. 2018;96:392-410.
6. Sansaniwal SK, Pal K, Rosen MA, Tyagi SK. Recent advances in the development of biomass gasification technology: a comprehensive review. *Renew Sustain Energy Rev*. 2017;72:363-384.
7. Strzalka R, Schneider D, Eicker U. Current status of bioenergy technologies in Germany. *Renew Sutain Energy Rev*. 2017;72:801-820.
8. Basu P. *Biomass Gasification, Pyrolysis and Torrefaction*. 3rd ed. Amsterdam: Elsevier; 2018.
9. Zang G, Jia J, Shi Y, Sharma T, Ratner A. Modeling and economic analysis of waste tire gasification in fluidized and fixed bed gasifiers. *Waste Manag*. 2019;89:201-211.
10. Yang K, Zhu N, Ding Y, Chang C, Wang D, Yuan T. Exergy and exergoeconomic analyses of a combined cooling, heating, and power (CCHP) system based on dual-fuel of biomass and natural gas. *J Clean Prod*. 2019;206:893-906.
11. Maneerung T, Li X, Li C, Dai Y, Wang C-H. Integrated downdraft gasification with power generation system and gasification bottom ash reutilization for clean waste-to-energy and resource recovery system. *J Clean Prod*. 2018;188:69-79.
12. Segurado R, Pereira S, Correia D, Costa M. Techno-economic analysis of a trigeneration system based on biomass gasification. *Renew Sustain Energy Rev*. 2019;103:501-514.
13. Taheri MH, Mosaffa AH, Garousi Farshi L. Energy, exergy and economic assessments of a novel integrated biomass based multigeneration energy system with hydrogen production and LNG regasification cycle. *Energy*. 2017;125:162-177.
14. Casas-Ledon Y, Spaudo F, Arteaga-Perez LE. Exergoenvironmental analysis of a waste-based integrated combined cycle (WICC) for heat and power production. *J Clean Prod*. 2017;164:187-197.
15. Zang G, Tejasvi S, Ratner A, Lora ES. A comparative study of biomass integrated gasification combined cycle power systems: performance analysis. *Biores Technol*. 2018;255:246-256.
16. Razak AMY. *Industrial Gas Turbines- Performance and Operability*. Cambridge: Woodhead Publishing Limited; 2007.
17. Al-Khori K, Bicer Y, Koç M. Integration of solid oxide fuel cells into oil and gas operations: needs, opportunities, and challenges. *J Clean Prod*. 2020;245:118924.
18. Rokni M. Design and analysis of a waste gasification energy system with solid oxide fuel cells and absorption chillers. *Int J Hydrogen Energy*. 2018;43:5922-5938.
19. Jia J, Abudula A, Wei L, Sun B, Shi Y. Thermodynamic modeling of an integrated biomass gasification and solid oxide fuel cell system. *Renew Energy*. 2015;81:400-410.
20. Arsalis A. A comprehensive review of fuel cell-based micro-combined-heat-and-power systems. *Renew Sustain Energy Rev*. 2019;105:391-414.
21. Borji M, Atashkari K, Ghorbani S, Nariman-Zadeh N. Parametric analysis and Pareto optimization of an integrated autothermal biomass gasification, solid oxide fuel cell and micro gas turbine CHP system. *Int J Hydrogen Energy*. 2015;40:14202-14223.
22. Ghaffarpour Z, Mahmoudi M, Mosaffa AH, Garousi Farshi L. Thermoeconomic assessment of a novel integrated biomass based power generation system including gas turbine cycle, solid oxide fuel cell and Rankine cycle. *Energ Conver Manage*. 2018;161:1-12.
23. Jia J, Abudula A, Wei L, Sun B, Shi Y. Effect of operating parameters on performance of an integrated biomass gasifier, solid oxide fuel cells and micro gas turbine system. *Biomass Biomassenergy*. 2015;75:35-45.
24. Bang M, Rokni M, Elegaard B. Exergy analysis of optimization of a biomass gasification, solid oxide fuel cell and micro gas turbine hybrid system. *Energy*. 2011;36(8):4740-4752.
25. Deng J, Wang RZ, Han GY. A review of thermally activated cooling technologies for combined cooling, heating and power systems. *Prog Energy Combust Sci*. 2011;37:172-203.
26. Çengel YA, Boles MA. *Thermodynamics*. 8th ed. New York: McGraw-Hill Education; 2015.
27. Ebrahimi K, Jones GF, Fleischer AS. Thermo-economic analysis of steady state waste heat recovery in data centers using absorption refrigeration. *Appl Energy*. 2015;139:384-397.
28. Wang RZ, Oliveira RG. Adsorption refrigeration—an efficient way to make good use of waste heat and solar energy. *Prog Energy Combust Sci*. 2006;32:424-458.
29. Wang J, Ma C, Jing W. Thermodynamic analysis of a combined cooling, heating and power system based on solar thermal biomass gasification. *Appl Energy*. 2019;247:102-115.
30. Moussawi HA, Fardoun F, Louahlia H. 4-E based optimal management of a SOFC-CCHP system model for residential applications. *Energy Convers Manag*. 2017;151:607-629.
31. Zhong L, Yao E, Dang Z, Hu Y, Zou H, Xi G. Conceptual design and performance analysis of a novel CHP system integrated with solid oxide fuel cell and supercritical CO2 partial preheating cycle. *Int J Energy Res*. 2021;45:3801-3820. https://doi.org/10.1002/er.6033.
32. Roy D, Samant S, Ghosh S. Performance assessment of a biomass fuelled advanced hybrid power generation system. *Renew Energy*. 2020;162:639-661.
33. Jia J, Shu L, Zang G, Xu L, Abudula A, Ge K. Energy analysis and techno-economic assessment of a co-gasification of woody biomass and animal manure, solid oxide fuel cells and micro gas turbine hybrid system. *Energy*. 2018;149:750-761.
34. Jayah TH, Aye L, Fuller RJ, Stewart DF. Computer simulation of a downdraft wood gasifier for tea drying. *Biomass Bioenergy*. 2003;25(4):459-469.

35. Prokash CR, Amitava D, Niladri C. Modelling of a downdraft biomass gasifier with finite rate kinetics in the reduction zone. *Int J Energ Res*. 2009;33(9):833-851.
36. Salem AM, Paul MC. An integrated kinetic model for downdraft gasifier based on a novel approach that optimises the reduction zone of gasifier. *Biomass Bioenergy*. 2018;109:172-181. https://doi.org/10.1016/j.biombioe.2017.12.030.
37. Jia J, Abudula A, Wei L, Shi Y. Performance comparison of three solid oxide fuel cell power systems. *Int J Energ Res*. 2013;37(14):1821-1830.
38. Jia J, Abudula A, Wei L, Jiang R, Shen S. A mathematical model of a tubular solid oxide fuel cell with specified combustion zone. *J Power Sources*. 2007;171(2):696-705.
39. Jia J, Jiang R, Shen S, Abudula A. Effect of operation parameters on performance of tubular solid oxide fuel cell. *AICHE J*. 2008;54(2):554-564.
40. Moran MJ, Shapiro HN, Boettner D, Bailey MB. *Fundamentals of Engineering Thermodynamics*. 8th ed. Hoboken: John Wiley & Sons; 2014.
41. Dincer I, Kanoglu M. *Refrigeration System and Applications*. 2nd ed. Chichester: John Wiley & Sons; 2010.
42. Dincer I, Rosen MA. *Exergy: Energy, Environment and Sustainable Development*. 2nd ed. London: Elsevier; 2012.
43. Szargut J. *Exergy Method: Technical and Ecological Applications*. Boston: WIT Press; 2005.
44. Wu B, Zhang X, Shang D, Di Bao SZ, Zheng T. Energetic-environmental-economic assessment of the biogas system with three utilization pathways: combined heat and power, biomethane and fuel cell. *Bioresour Technol*. 2016;214:722-728.
45. Borello D, De Caprariis B, De Filippis P, Di Carlo A. Thermo-economic assessment of a olive pomace gasifier for cogeneration applications. *Energy Procedia*. 2015;75:252-258.
46. Elsner W, Wysocki M, Niegodajew P, Borecki R. Experimental and economic study of small-scale CHP installation equipped with downdraft gasifier and internal combustion engine. *Appl Energy*. 2017;202:213-227.
47. Sorace M, Gandiglio M, Santarelli M. Modeling and techno-economic analysis of the integration of a FC-based micro-CHP system for residential application with a heat pump. *Energy*. 2017;120:262-275.
48. Giarola S, Forte O, Lanzini A, Gandiglio M, Santarelli M, Hawkes A. Techno-economic assessment of biogas-fed solid oxide fuel cell combined heat and power system at industrial scale. *Appl Energy*. 2018;211:689-704.
49. Zang G, Jia J, Tejasvi S, Ratner A, Lora ES. Techno-economic comparative analysis of biomass integrated gasification combined cycles with and without CO_2 capture. *Int J Greenhouse Gas Control*. 2018;78:73-84.
50. Bellos E, Tzivanidis C, Symeou C, Antonopoulos k A. Energetic, exergetic and financial evaluation of a solar driven absorption chiller - a dynamic approach. *Energ Conver Manage*. 2017;137:34-48.

How to cite this article: Jia J, Zang G, Paul MC. Energy, exergy, and economic (3E) evaluation of a CCHP system with biomass gasifier, solid oxide fuel cells, micro-gas turbine, and absorption chiller. *Int J Energy Res*. 2021;45:15182–15199. https://doi.org/10.1002/er.6794